JOURNAL OF Materials CHEMISTRY

Thin film deposition: a novel synthetic route to new materials†

Bernard Mercey,* Paul A. Salvador, Wilfrid Prellier, Trong-Duc Doan, Jérôme Wolfman, Jean-François Hamet, Maryvonne Hervieu and Bernard Raveau

Laboratoire CRISMAT-ISMRA UMR 6508, 6, Bd. du Maréchal Juin, 14050 Caen, Cedex, France. E-mail: mercey@crismat.ismra.fr

Received 23rd April 1998, Accepted 29th June 1998

In this paper, we discuss the utility of thin film deposition as a synthetic approach to the realization of new oxide materials. Thin film deposition has been shown previously to be well suited to stabilizing both highly metastable phases and superlattices having unique atomic order which are not attainable *via* classical preparatory routes. That this approach is only in the early stages of realizing its full potential as a synthetic method is demonstrated using classical pulsed laser deposition to grow new, artificially layered materials. Superlattices of metastable copper and manganese oxides having perovskite-like sub-cells were grown; they have the nominal formulae $(La_{0.8}Ba_{0.2}CuO_{2.6\pm x})_m(SrCuO_{2+\delta})_n$ and $(LaMnO_3)_m(A'MnO_3)_n$ (A' = Sr and Y). Superlattice reflections are observed in the X-ray diffraction spectra, indicative of a two-dimensional cationic order not observed in bulk materials of similar stoichiometries. Moreover, the chemistry of the dimensionally confined layers in the superlattices differs from that of similar 'bulk-like' materials. Anomalous CMR effects are presented for the $(LaMnO_3)_m(SrMnO_3)_n$ superlattices, demonstrating that new and unique physical properties are attainable *via* this particular synthetic approach. We also discuss the structure and growth mode of single films of $LaMnO_3$ with respect to superlattice formation.

1. Introduction

1.1. Thin film synthesis of materials

The earliest application of thin film deposition methods was to modify the surface characteristics of a material by depositing upon it a very thin layer of a different material.[1] Soon after, thin film deposition methods were exploited to attain materials in other technologically useful forms. Upon the development of molecular beam epitaxy (MBE) techniques, it was shown that the growth of very thin layers could be precisely controlled in a highly reproducible fashion,[2] and this has opened the route for the growth of fascinating new materials. Semiconductor superlattices built up from the alternation of extremely thin layers of gallium arsenide and aluminium arsenide are examples of such materials which have been extensively investigated.[2] It is important to note that such stacking sequences are impossible to attain *via* the classical synthetic routes of solid state chemistry.

One of the most important events to have aided the development of oxide thin film growth was the realization of the first high-temperature superconducting oxide thin film,[3] because, at that time, the most sophisticated thin film deposition methods were not well suited to the growth of oxide materials. The possibility of using oxides for advanced and exotic technological applications has given rise to a large body of important work aimed at adapting thin film deposition systems for oxide growth. The diverse physical properties exhibited by oxide materials make them attractive candidates for thin film growth from both technological and scientific perspectives.[4,5]

From the synthetic perspective, thin film growth is interesting because it allows one to prepare phases (particularly oxides) which are normally stable only under extreme conditions of temperature and pressure, or even materials stable only as films.[2,6–18] A particularly exciting subset of the latter materials are tailored oxide superlattices and 'artificial' structures. Three significant features required of a thin film technique used for new materials synthesis are: (i) a high level of control over complex stoichiometries, both cationic and anionic; (ii) a temperature reduction from standard synthesis conditions, which leads to different thermodynamic/kinetic control over the reaction products; (iii) epitaxial growth on the underlying terminating surface, this can be either a substrate or a previously deposited film. While the emphasis of this article will be on pulsed laser deposition (PLD), we will first review the usefulness of various other deposition techniques in the following section before exploring in depth PLD as an emerging tool for the synthesis of advanced materials.

1.2. Applicability of various thin film techniques to new materials synthesis

Amongst the various thin film deposition methods used for the growth of oxides, only a very small number are used for the growth of new phases or of tailored oxide superlattices. The most important feature that the methods we shall consider have in common is the ability to achieve and control complex film stoichiometries. Thus, MOCVD has not been extensively used for new materials synthesis because of the great dependence of the film stability on the metal–organic precursors and the deposition conditions. A major focus with this technique is attaining appropriate precursors for phase stabilization and a major drawback is that the variation of sources between runs can be difficult to achieve in practice. Similarly, the dependence on precursor chemistry in atomic layer epitaxy (ALE), a technique with potential in structural engineering on the atomic/monolayer scale, has limited its extensive application towards complex, new (oxide) materials growth.[17]

From the viewpoint of easily and accurately controlling the film stoichiometry, sputtering deposition methods, which allow deposition on very large areas, are generally poor methods for new materials synthesis because they do not ensure a direct stoichiometry correspondence between the target and the film. Nevertheless, several groups have used this method to grow both metastable phases, such as $SrCuO_2$ and $CaCuO_2$,[19–21] and oxide superlattices, such as $(Sr_{1-x}Ca_xCuO_2)_m$ $(Sr_{1-x}Ca_xRuO_3)_n$,[22] $(PrBa_2Cu_3O_{7-\delta})_m(YBa_2Cu_3O_{7-\delta})_n$,[23–26] $(BiSr_2CuO_y)_m(CaCuO_2)_n$,[27,28] and $(Ba_2CuO_2CO_3)_m$-

†Basis of the presentation given at Materials Chemistry Discussion No. 1, 24–26 September 1998, ICMCB, University of Bordeaux, France.

$(CaCuO_2)_n$. [11,29] Extreme care must be taken in each case with respect to the deposition conditions (pressure, target substrate distance, plasma gas composition, *etc.*) because small variations can often lead to large variations in the overall film composition. While these results demonstrate that oxide films having desirable structural qualities and physical properties can be attained *via* sputtering, its poor adaptability and lack of compositional control make reactive sputtering very difficult to use as a convenient route for new material synthesis.

Deposition methods which allow for very precise control of the deposited species are the best candidates for new material synthesis. Molecular beam epitaxy (MBE), suitably modified to achieve complete oxidation of the growing film, is certainly the most accurate method to control the composition and spatial arrangement of the deposited species.[30] There are, however, two features of this technique which make it a difficult method to use practically in the search of new materials. The first drawback is the expense: not only is the initial set-up cost of this method considerably expensive, but the continual operational costs are also very high. The second drawback is that MBE is pragmatically a difficult and time consuming experiment even for semiconducting materials, and it is rendered yet more complicated by the presence of oxidants which can react with the metal sources and modify the deposition rates of the corresponding metals. Therefore, MBE systems optimized for the deposition of oxide films must have permanent, *in-situ* control of the atomic flux from each effusion cell.[31]

Nevertheless, MBE has been shown to be an extremely powerful method of growing oxide thin films with well controlled stoichiometries and monolayer-smooth surfaces/interfaces. Several groups have successfully used this technique to deposit very thin films of $REBa_2Cu_3O_{7-\delta}$, RE = rare earth cation.[8,32–34] The possibilities of preparing novel materials by the MBE method are demonstrated nicely by the work of Dr Sato's group,[35] in which a new superconducting phase was prepared in the Ba–Cu–O system; the critical temperature was close to 40 K and the structure was similar to that of La_2CuO_4. The incredible potential of this deposition method to realize tailored oxide materials, is illustrated by the tremendous work of the Varian group,[8,9] who, using deposition apparatus specially designed for the controlled, layer-by-layer growth of oxide materials, have achieved several important results on artificially layered structures. In a study of the superconducting behavior of cuprates containing bismuth, it was demonstrated that the superconducting properties are highly dependent upon the particular layer stacking sequence. Superconductor–insulator–superconductor (S–I–S) junctions were also successfully prepared using this precisely controlled growth method.[36] More recently, manganese oxide materials have also been grown by the same group.[37] The precise control of the growth conditions enabled by the MBE technique is of importance for the magnetic study of these manganese oxides since it has been demonstrated that small changes in composition may induce very large variations in the magnetic properties of the films. Superlattice structures of $(BaTiO_3)_m(SrTiO_3)_n$ were also obtained using MBE.[30]

Because of the experimental complexity of successful oxide–MBE deposition techniques, it is interesting to investigate other methods which allow for a comparable level of control over film stoichiometries and spatial arrangements. Although the standard pulsed laser deposition (PLD) method is relatively simple experimentally (and we will focus on in the following sections), it cannot achieve such accurate control over the flux of species as that of the MBE method. The level of control afforded during growth in PLD can be drastically increased using a modified deposition system, while the level of experimental complexity remains relatively simple. *In-situ* RHEED (reflection high energy electron diffraction) can be used with PLD, when the deposition pressure is greatly reduced from standard PLD conditions (to 10^{-3}–10^{-4} mbar from 0.3 mbar) to decrease the importance of electron scattering by the background gas molecules.[13,14,30,38–43] In this relatively low pressure range, the activity of molecular oxygen is not high enough to promote the complete oxidation of the growing film, and stronger oxidizers, such as N_2O, NO_2, O_3, or atomic oxygen, are required.[14] The growth control provided by the RHEED-equipped PLD system combined with the relative simplicity of PLD renders this new deposition method very attractive for solid state chemists. It allows for the growth of tailored inorganic structures, as exemplified by the growth of $AECuO_2$ [AE = Ba, Sr, Ca] and various superlattices of these phases,[38,41,42,44–47] $(BaAuO_x)(BaCuO_{2+y})(CaCuO_2)_n$ superlattices,[48,49] and $(SrVO_3)_m(SrTiO_3)_n$ superlattices.[43]

1.3. Classical pulsed laser deposition of new materials

1.3.1 Single material films. Standard pulsed laser deposition (PLD) is relatively uncomplicated experimentally and usually leads to an excellent correspondence between the target and film stoichiometries. This and the lack of required complex oxidation reactions during film crystallization have made PLD the most popular method for thin film deposition of oxide materials.[13,14,50] These attractive features arise from the fact that most PLD experiments are conducted with sintered targets having the same stoichiometry, and in many cases similar crystal structures, to those of the films. Despite the rather crude control of the deposition rate afforded by standard PLD systems, this uncomplicated technique generally yields excellent reproducibility of both the obtained thickness and physical properties of the deposited films.

Two features which are potential limiting factors to the widespread technological applicability of the PLD method must be considered. First, homogeneous deposition over very large areas is difficult to achieve (particulary for complex oxides) since the ablated species are concentrated within a very small solid angle; thus a displacement of the substrate or a change in the direction of the ablated species is required to overcome this limitation. The second feature is related to the ablation mechanism: owing to the extremely high energy density dissipated on the target surface, large particles are often ejected from the target and may stick to the substrate/film surface. These large particles resemble droplets and are a problem for either device or superlattice realization since they both require growth of sequential layers whose electrical or crystalline quality can be degraded by such droplets. This problem can be partially overcome by changing the deposition set up to an off-axis geometry, mechanically blocking the arrival of large particles at the substrate surface, and/or using highly dense targets and carefully tuning the laser beam energy.

It is somewhat surprising that PLD has not been used more extensively for the growth of new materials: single films of 'classical' superconducting cuprates or manganese oxides are routinely grown (and superlattices built up from well known materials are also synthesized),[13,51–54] but there are only a few papers in the emerging area concerned with the growth of materials having new compositions or structures. For example, by taking advantage of the flexibility of PLD and using a multi-target system, Gupta *et al.*[55] were able to completely describe the phases in the Sm–Sr–Cu–O system as thin films. Desfeux *et al.*[56] deposited a cubic perovskite phase having the composition $La_4BaCu_5O_{13\pm x}$ and although the film does not adopt the complex structure of the bulk material[57] their metallic electrical properties are rather similar. Allen *et al.*[58] prepared a new superconducting material having a critical temperature of 76 K by depositing a film from a $Ba_2Ca_3Cu_5O_x$ target under a gas mixture containing oxygen and carbon dioxide. These films can be described as the intergrowth of structural blocks containing carbonate groups with blocks having the 'infinite layer'-type structure: $(Ba_2CuO_2CO_3)_n$-

$(CaCuO_2)_m$. Although these films were grown from a single target, they are comprised of numerous intergrowth phases corresponding to members of the above-mentioned family having $n=1$ while m varies between 1 and 7.[58]

Although a large amount of oxide PLD research has been focused on copper-based systems, because of their obvious scientific interest and the benefits two dimensional growth techniques offer for the synthesis of layered cuprates,[8,9] the use of PLD as a synthetic tool to attain novel materials is by no means limited to the copper oxide systems. We have recently shown that while $YMnO_3$ adopts a non-close packed, hexagonal structure under ambient synthetic conditions, the PLD synthesis of this phase on perovskite-like substrates favors the epitaxial growth of a perovskite-like material (similar to the high-pressure perovskite form of $YMnO_3$).[18] This is completely analogous to the stabilization of the 'infinite-layer' type phases in the copper oxide systems, which are usually only stable in bulk form when synthesized under extreme pressure conditions.

1.3.2 Superlattice growth. In addition to metastable single material films, spatial confinement of different materials into distinct layers can be achieved using sequential deposition in this standard PLD approach. The classical PLD method has been used for the growth of these types of tailored superlattices, and is successful because the deposition rate remains sufficiently constant between experiments. To grow superlattices exhibiting good structural properties, the deposition rate should be kept at a relatively small value, *i.e.*, $\leqslant 0.5$ Å per laser pulse, and this can usually be attained by a slight decrease in the deposition pressure from standard conditions (the latter often having deposition rates of >1 Å per laser pulse). Low deposition rates generally reduce film surface roughness, thereby increasing the surface or interfacial quality of the films, and enable a better control of the thickness (or absolute layer coverage) of the deposited layer.

The infinite-layer based superlattices, $(AECuO_2)_m$-$(AE'CuO_2)_n$ (AE = alkaline earth metal), have been the most extensively investigated artificial structures grown *via* classical PLD.[12,59–61] Tailored superlattices belonging to the oxycarbonate family discussed above, *i.e.*, $(Ba_2CuO_2CO_3)_m(AECuO_2)_n$, were synthesized wherein the m and n values were fixed by the alternation sequence to correspond to a single member of the family.[62] In the field of ferroelectrics, $(SrTiO_3)_m(BaTiO_3)_n$[63,64] superlattices displayed dielectric properties which differed vastly from films having similar stoichiometries but no superlattice structure. Superlattices of $(KTaO_3)_m(KNbO_3)_n$[65] and $(Y_3Fe_5O_{12})_m(Gd_3Ga_5O_{12})_n$[66] have also been stabilized using a classical PLD approach.

1.4. New directions

While the above results demonstrate that thin film deposition has a great potential for impacting materials synthesis and structural design, many questions remain to be addressed as to its general utility in this area. In the remainder of this article we attempt to address some of the issues that challenge PLD thin film growth as a synthetic method for obtaining new materials. This is discussed with respect to the realization of novel two dimensional cationic order in the $Ln_{1-x}AE_xBO_{3-\delta}$ systems, where Ln = La or Y, AE = Ba, Sr, or Ca, and B = Cu or Mn. In each of the chosen cases, standard synthetic conditions lead to random (or at least non-layered) distributions of the A cations over crystallographically equivalent sites. Since the physical properties are strongly dependent on cationic order in the copper and manganese oxide materials, new types of cationic order may indeed lead to new and interesting physical properties.

The growth of $(La_{0.8}Ba_{0.2}CuO_{2.6\pm x})_m(SrCuO_{2+\delta})_n$ is investigated and compared with that of $(La_{0.8}Ba_{0.2}CuO_{2.6\pm x})_m$-$(CaCuO_2)_n$ and $(CaCuO_2)_m(SrCuO_2)_n$. The realization of the first two stacking sequences may lead to a structure having two-dimensional CuO_2 networks, a first requirement for superconductivity, interleaved by a metallic region in which the carrier concentration can be controlled *via* oxygen intercalation/de-intercalation, a very favorable structural motif for high-T_c superconductivity.[5,67,68] It is important to recall that films of $La_4BaCu_5O_{13\pm x}$ were found to be metallic with a simple cubic perovskite structure,[56] hence the formula $La_{0.8}Ba_{0.2}CuO_{2.6\pm x}$. Layered cuprates often have structures where concerted cationic- and oxygen-vacancy order leads to a two-dimensional electronic state; the bulk compounds in the $(La,Ba,Sr)CuO_{3-x}$ system lack the two-dimensional A-site order and the concerted order between cations and anions leads to a three dimensional electronic state.[57,69–72] We are interested in determining if induced two dimensional cationic order may lead to two dimensional electronic properties and superconductivity. The importance of the interfacial chemistry in the artificially layered materials is demonstrated, herein, and discussed with respect to the stability of particular films.

The growth of manganese oxides having artificial cation order was also investigated in the systems $(LaMnO_3)_m$-$(A'MnO_3)_n$, where A' = Y, Sr, to demonstrate the applicability, utility, and potential of PLD as a synthetic tool for materials synthesis and structural engineering. Although the benefits of obtaining two-dimensional cationic order may not be immediately evident in the manganese oxides, the close relationships between charge, orbital, magnetic and structural order in these compounds implies that novel properties may exist in these regions. Moreover, it was recently shown that a unique synthetic approach allowed for the synthesis of ordered, layered (as well as disordered) A-site bulk materials having the stoichiometry $LaBaMn_2O_6$, and that the colossal magnetoresistant (CMR) behavior was strongly dependent on the cationic order.[73] Thus, it is interesting to demonstrate that artificial A-site order can be attained using the end-member compounds such as $YMnO_3$, $LaMnO_3$, and $SrMnO_3$, to extend our ability to explore the structure–property relationships in novel compounds. We will discuss preliminary results in the growth and XRD characterization of several superlattices of this type, along with the challenges remaining to tailor successfully the atomic structures of materials using PLD. The stabilities of different phases and their growth modes on certain substrates are also discussed, and the important chemical effects of the artificial order on the structural stability of these materials are demonstrated.

2. Experimental

Dense ceramic targets having the nominal formulae (with our abbreviation scheme following in parentheses) $La_{0.8}Ba_{0.2}CuO_{2.6\pm\delta}$ (LBCO), $SrCuO_2$ (SCO), $CaCuO_2$ (CCO), $YMnO_3$ (YMO), $LaMnO_3$ (LMO), and $SrMnO_3$ (SMO) were synthesized *via* standard ceramic synthesis methods. Appropriate ratios of La_2O_3, Y_2O_3, $BaCO_3$, $SrCO_3$, $CaCO_3$, CuO and MnO_2 powders were mixed and intimately ground using a semi-planetary ball mill. For the copper-oxide targets, the powder was annealed twice for 12 h at 900 °C and once for 12 h at 950 °C, with intermediate grindings. For the manganese oxide targets, the powder was annealed twice for 12 h at 900 °C and once for 12 h at 1200 °C, with intermediate grindings. Pellets having a diameter of 2.5 cm were cold uniaxially pressed and sintered for 12 h at 950 °C or 1500 °C for the copper oxides and manganese oxides, respectively.

The PLD apparatus used for deposition is described elsewhere.[18,56,58,62] Some of the important deposition parameters are: $\lambda = 248$ nm (KrF), pulse rate = 3 Hz, laser power density = 1–2 J cm^{-2}, target to substrate distance = 47–50 mm. Optical quality single-crystal substrates of (100) $SrTiO_3$, (100) $LaAlO_3$, and (110) $NdGaO_3$ were ultrasonically cleaned in acetone and then in alcohol, and were attached to the heater

using silver paste. A type K thermocouple was mechanically attached to the heater block close to the substrates and the temperature measured at this location is referred to as the deposition temperature. The background pressure of the chamber was 10^{-5} mbar. During deposition, the substrates were held at a constant temperature ranging from 580 to 725 °C in a dynamic vacuum having an O_2 pressure ranging from 0.10 to 0.60 mbar. After deposition was completed, the oxygen pressure was increased to a static value of 200–500 mbar, and the films were cooled to room temperature at 20 °C min^{-1}. Further details of depositions are given below alongside the discussion of the corresponding films.

Superlattice films were deposited by alternating the number of laser pulses in an appropriate manner according to the deposition rate of each material. The deposition rate was observed to be relatively constant when identical deposition parameters are used, but important differences occur upon changing these parameters. Thus, the rate must be verified under each set of conditions. The simplest manner of calibration is to deposit several superlattices and to determine the thickness of each layer and the overall superperiod from the satellite peak positions, as discussed below. This gives a fairly accurate deposition rate under the conditions of superlattice growth.

X-Ray diffraction was carried out using a Seiffert XRD 3000 diffractometer with Cu-Kα_1 radiation. Transmission electron microscopy (TEM) was carried out using a JEOL 200 CX microscope, equipped with an energy-dispersive spectroscopy (EDS) analyzer (Kevex) to determine the film stoichiometry. Films were also observed using a Philips XL30 FEG scanning electron microscope (SEM) coupled with EDS (Oxford) to observe their microstructural quality and compositional homogeneity.

Electrical leads were attached using indium solder to evaporated silver contacts on select copper oxide superlattices. Four-point resistance measurements were carried out as a function of temperature. Contacts were made to the manganese oxide superlattices using ultrasonically diffused indium, and leads were attached with gold wires. Temperature-dependent, four-point resistance measurements were performed using a Quantum Design PPMS in applied magnetic fields of up to 7 T.

3. Results and discussion

3.1. Application of PLD for the synthesis of new copper oxides

A standard synthetic starting point for the growth of superlattices and artificial structures is to find overlapping deposition conditions for each of the films where the growth rates afford appropriate control and proper surfaces. The importance of this step will be discussed below, as this approach ignores chemical effects associated with the dimensional confinement of different phases. LBCO, CCO, and SCO could be stabilized as single epitaxial films on $SrTiO_3$ substrates in a temperature window of 580–680 °C using deposition pressures between 0.1 and 0.5 mbar O_2, respectively. For LBCO, one must find deposition conditions which promote the growth of the disordered cubic perovskite LBCO phase in the absence of a secondary La_2CuO_4-type phase. For CCO, the crystalline quality, as judged by the diffraction spectra, was increased at higher deposition temperatures. SCO films were found to exhibit good crystallinity and corresponded to the structure expected for the $SrCuO_2$ stoichiometry, *i.e.* having no excess oxygen, over the entire range of deposition conditions listed above. Poorly crystallized phases of $SrCuO_{2+\delta}$ were found at lower temperatures.

Thus, $(SCO)_m(CCO)_n$ superlattices were grown and characterized, and we obtained results similar to those reported previously. Fig. 1 shows the diffraction spectra of a $[(SCO)_4(CCO)_3]\times 50$ (the latter number indicates the number of deposition cycles) superlattice grown at 640 °C under 0.2 mbar O_2. The deposition rates for both materials were near 0.20–0.25 Å per pulse. The superlattice period is calculated using the formula:[74]

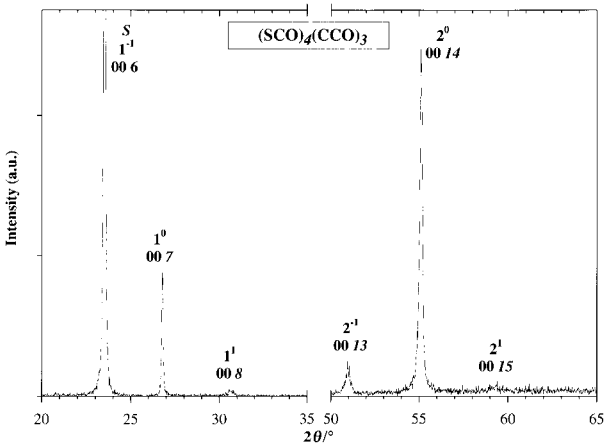

Fig. 1 X-Ray diffraction pattern of the $[(SrCuO_2)_4(CaCuO_2)_3]\times 50$ superlattice film. Intensity is given in arbitrary units. Peaks are indexed according to Schuller's notation (see text) and, alternatively, on an expanded unit cell having $c=7a_p$. The peak from the [100]-$SrTiO_3$ substrate are denoted with *S*.

$$\Lambda = \frac{\lambda}{2(\sin\theta_n - \sin\theta_{n-1})} \quad (1)$$

where Λ corresponds to the superperiodicity, λ is the wavelength, and θ_n and θ_{n-1} correspond to the diffraction angle of two consecutive peaks of the superlattice. The theoretical parameter calculated for this stacking sequence is 23.27 Å ($4\times 3.432+3\times 3.181$), and this is well matched to the observed value of 23.3 Å.

The peaks in Fig. 1, and in the diffractograms which follow, are indexed according to Schuller's notation.[75] For example, the principle second order peak is denoted 2^0, while the first satellite peaks at higher and lower angles of this peak of the film are denoted as 2^1 and 2^{-1}, respectively. It should be noted that these *c*-axis oriented films can also be indexed on a larger crystallographic cell corresponding to the superlattice repeat unit. In the case of the $(SCO)_4(CCO)_3$ superlattice the new repeat unit is *ca.* $7a_p$ (a_p corresponds to the simple perovskite lattice parameter) in the direction of the substrate normal. This leads to an equivalent indexing of the 00*l* lines as $l=6$, 7, 8, 13, 14, and 15 for the 1^{-1}, 1^0, 1^1, 2^{-1}, 2^0, and 2^1 peaks, respectively (see Fig. 1).

The X-ray diffraction diagrams of two $(LBCO)_m(SCO)_n$ samples are shown in Fig. 2 and 3 and evidence the growth of superlattices: satellite peaks are clearly seen on both sides of the second primary Bragg peak (*i.e.*, the 2^0 reflection). The intensities of the 1^0 peak and its associated superlattice peaks are always observed to be of much lower intensity than the second order peaks for these superlattices. The superlattice parameter, calculated from the X-ray data in Fig. 2 and using eqn. (1), is 26.7 Å, for a superlattice of the nominal formula $[(LBCO)_3(SCO)_4]\times 45$. The theoretical parameter calculated for this stacking sequence is 25.3 Å ($3\times 3.86+4\times 3.43$), but this is not well matched to the observed value. However, if one uses the *c*-parameter reported for an oxygen-rich 'infinite-layer' block, *i.e.*, $SrCuO_{2+\delta}$,[41,47] the theoretical parameter is 26.2 Å ($3\times 3.86+4\times 3.65$), and this is in much closer agreement with the observed values. Similar results were obtained for an $m=3$, $n=2$ superlattice, $[(LBCO)_3(SCO)_2]\times 50$, as shown in Fig. 3: the observed and theoretical values match well, 19.2 Å and 18.9 Å respectively, when one considers the 'infinite-layer' block as being oxygen rich (*i.e.*, $SrCuO_{2+\delta}$). We will call this oxygen-rich phase (SCO+δ), and thus

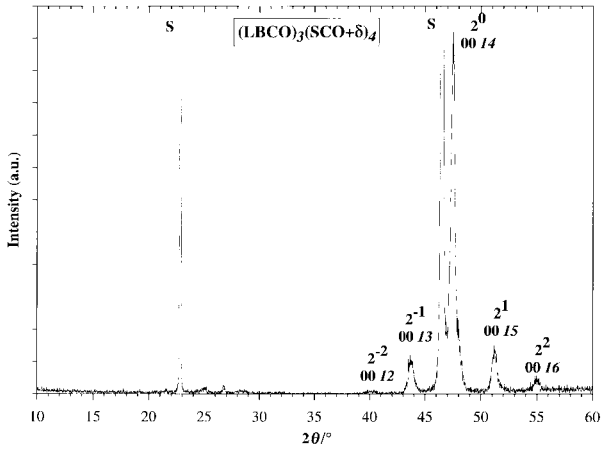

Fig. 2 X-Ray diffraction pattern of the $[(La_{0.8}Ba_{0.2}CuO_{2.6\pm x})_3(SrCuO_{2+\delta})_4]\times 45$ superlattice film. Intensity is given in arbitrary units. Peaks are indexed according to Schuller's notation (see text) and, alternatively, on an expanded unit cell having $c=7a_p$. The peaks from the [100]-$SrTiO_3$ substrate are denoted with *S*.

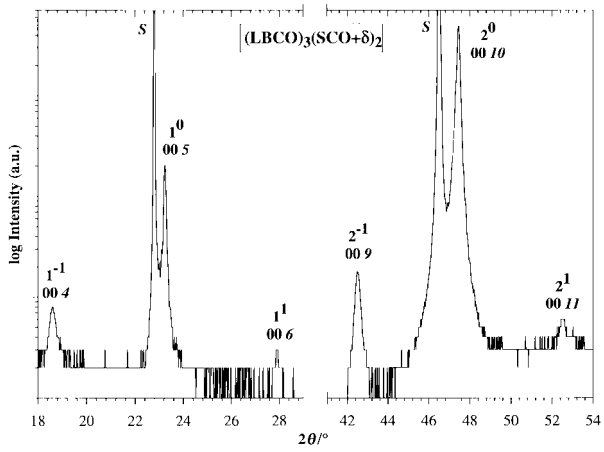

Fig. 3 X-Ray diffraction pattern of the $[(La_{0.8}Ba_{0.2}CuO_{2.6\pm x})_3(SrCuO_{2+\delta})_2]\times 50$ superlattice film. Intensity is given on a logarithmic scale in arbitrary units. Peaks are indexed according to Schuller's notation (see text) and, alternatively, on an expanded unit cell having $c=5a_p$. The peaks from the [100]-$SrTiO_3$ substrate are denoted with *S*.

the obtained superlattices are more precisely $[(LBCO)_3(SCO+\delta)_4]\times 45$ and $[(LBCO)_3(SCO+\delta)_2]\times 50$, for the materials of Fig. 2 and 3, respectively.

An important question which needs to be addressed in superlattice stabilization is: what is the role of the interfacial chemistry (between the distinct layers) in the stabilization of particular structures? We will address this question further below with respect to manganese-based perovskite-like superlattices. With respect to the $(LBCO)_m(SCO+\delta)_n$ superlattices, this question can be rephrased as: what is the role of the excess oxygen in the stabilization of the observed $(LBCO)_m(SCO+\delta)_n$ superlattices? For example, under conditions identical to those used above for the $(LBCO)_m(SCO+\delta)_n$ superlattices, we obtained $(SCO)_m(CCO)_n$ superlattices wherein neither the $SrCuO_2$ nor the $CaCuO_2$ layers contained excess oxygen, and the superlattice peaks were well defined (in agreement with literature reports[21,42,59,60]). This result implies that the excess oxygen found in the $(LBCO)_m(SCO+\delta)_n$ superlattices is a consequence of the superlattice stacking arrangement itself, and not simply from the deposition conditions used. Furthermore, thick bilayer or trilayer films of LBCO and SCO that were deposited under identical conditions did not exhibit excess oxygen in the SCO layer.

The stability of these superlattices being related to the excess oxygen is further corroborated by the fact that we were unable to stabilize analogous $(LBCO)_m(CCO)_n$ superlattices using any of the deposition conditions given above. That $CaCuO_{2+\delta}$ has not been reported, except in extremely oxidizing conditions and at thicknesses corresponding to less than two unit cells,[47] may be the reason that these latter superlattices are unstable under these conditions. This hypothesis, however, requires further testing; in any case, the different architectures of these superlattices clearly control various aspects of their internal chemistry, such as their stabilities and oxidation preferences.

Fig. 4 presents the electrical behavior of these two superlattices grown under the above-given deposition conditions. The film with a thicker $SCO+\delta$ layer [Fig. 4(a)] exhibits semiconducting behavior over the entire temperature range while the LBCO rich film [Fig. 4(b)] exhibits weak metallic behavior over the temperature range from 50 to 200 K. Optimization of the carrier concentration, perhaps by *ex-situ* annealings, is clearly required to realize superconductivity. Of extreme importance, with respect to achieving superconductivity, is the stabilization of oxygen-stoichiometric SCO layers, because incorporation of oxygen between the copper–oxygen layers is often deleterious to superconductivity. The structural integrity of the two dimensional CuO_2 sheets may be perturbed owing to the incorporation of excess oxygen as well. Work is currently being conducted to understand the relationships between the deposition parameters and *ex-situ* annealing on the structure and properties of these artificially ordered materials. The important point demonstrated here is that two-dimensional cationic order, which is not attainable with standard synthetic

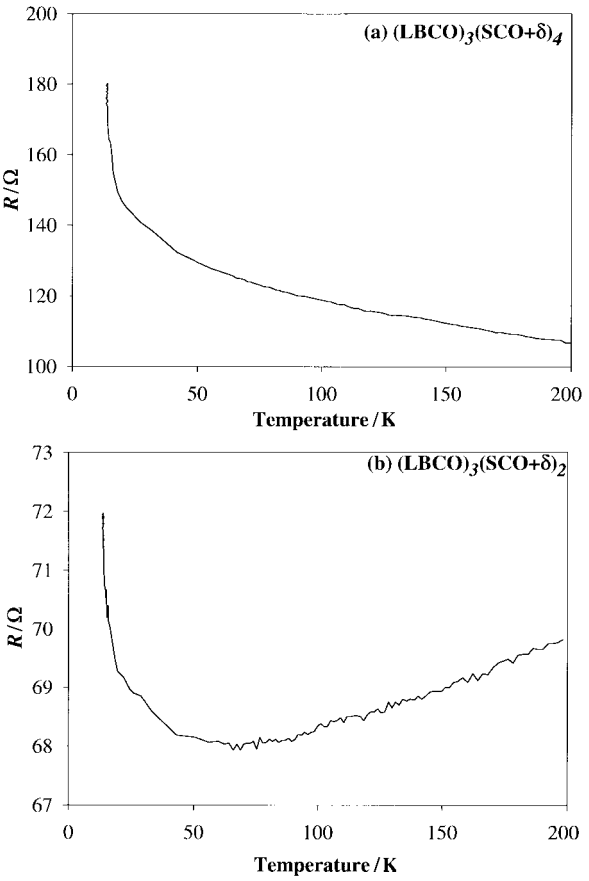

Fig. 4 Resistance, *R* (Ω), *vs.* temperature (K) for two LBCO/SCO superlattices. (a) The $(La_{0.8}Ba_{0.2}CuO_{2.6\pm x})_3(SrCuO_{2+\delta})_4$ material exhibits a weak semiconducting behavior in the 50–200 K temperature range. (b) The $(La_{0.8}Ba_{0.2}CuO_{2.6\pm x})_3(SrCuO_{2+\delta})_2$ material exhibits weak metallic behavior in the 50–200 K temperature range.

approaches, is achievable in the LBCO/SCO+δ system *via* PLD. However, as with most oxygen-nonstoichiometric layered cuprates, further work is necessary to optimize the carrier concentrations and structural properties to favor superconductivity.

3.2. Application of PLD for the synthesis of new manganese oxides

In order to attain two-dimensional cationic order in perovskite-like manganese oxides, we first investigated the growth of single material films. We have previously studied the stabilization of YMO and found that the surface roughness and growth rates of the epitaxial films were well within the regime for superlattice growth.[18] Thus we proceeded to investigate the region of stability for single materials films of both LMO and SMO.

A few reports on the stabilization of $La_{1-x}Mn_{1-y}O_3$ films (by various techniques) have been published previously,[76–79] and it is evident that the structure and resulting properties are closely related to the deposition conditions. Therefore, it is important to understand the growth modes and structures under various growth conditions if one is to use this material as a structural unit in manganese oxide superlattices having unique order on the perovskite A-site sublattice. We deposited films of $LaMnO_3$ under various conditions, and herein present the growth mode and crystal structure, on [110]-oriented $NdGaO_3$ substrates, and the implications these have for superlattice growth. The X-ray diffraction spectrum of a film deposited with a dynamic pressure of 0.4 mbar O_2, a deposition temperature of 650 °C, an energy density of 1 J cm^{-2}, and cooled in a static vacuum of 500 mbar O_2 is shown in Fig. 5. A sharp diffraction line of the film is observed just to the left of the 220 substrate peak at a d spacing of 1.949 Å, and this can be indexed (see below) as the 004 reflection of a rhombohedrally distorted perovskite-like cell, where $a=7.796$ Å$\approx 2a_p$. The shoulder observed to the left of the 110 substrate peak corresponds to the 002 reflection of the film. This implies that these films are highly oriented and have a single perovskite-like cell parameter perpendicular to the substrate plane. Similar results have been obtained for related films deposited by CVD, spray pyrolysis and laser ablation.[76–78,80]

In order to characterize further the crystal structure and to understand better the growth mechanisms, selected area electron diffraction (SAED), energy dispersive spectroscopy (EDS) and high resolution electron microscopy (HREM) were performed on a cross section of this film. EDS yielded a La/Mn ratio ≈ 1, indicating stoichiometric (within the experimental error of a few atom%) transfer from the target. Stoichiometric $LaMnO_3$ has a distorted perovskite cell and adopts an orthorhombic structure: cell parameters a, $b\approx(\sqrt{2})a_p$, $\sqrt{(2a_p)}$; $c\approx 2a_p$.[81,82] A SAED pattern from a cross section of this film is given in Fig. 6 and does not correspond to the pattern of an orthorhombic type cell, but rather appears to be a 'pseudocubic', simple perovskite cell. The sharpness of the diffraction spots attests to the high crystalline quality of the film. Close inspection of this SAED pattern shows a slight deviation of the angle between the c^* and a^* (or b^*) axes from 90°. This is in agreement with the space group $R\bar{3}c$, which has been observed previously for cation-substoichiometric materials (*e.g.*, $La_{1-x}Mn_{1-x}O_3$; $x\approx 0.05$),[81,82] and we have thus indexed the ED and X-ray patterns accordingly (using the alternate face centered cell to emphasize the relationships to the perovskite cell) with a doubled perovskite base-cell ($a_{film}=7.796$ Å$\approx 2a_p$).[81] The lattice parameters determined from the SAED are in agreement with that determined from the XRD data. This implies that the conditions used in the synthesis lead to a 'self-doped' film, *i.e.*, a mixture of Mn^{3+} and Mn^{4+}, owing to vacancies on the cationic sublattice. Previous investigations have shown that self-doped films exhibit CMR behavior,[42,76,78,80] and detailed physical property measurements will be published elsewhere.

The low-magnification image of this cross section is given in Fig. 7 and it reveals two interesting features. First, the growth mode of this perovskite-like phase is highly columnar, with a column height of *ca.* 3250 Å and a total film thickness of *ca.* 3500 Å. These columns are observed to be *ca.* 200 Å wide, each column presents identical orientations with respect to the substrate, and very little mosaic tilt is observed in the HREM image of each column. The second interesting feature explains the difference between the column height and total film thickness: one observes the existence of an interfacial layer at the substrate/film surface which is non-columnar in nature and is *ca.* 250 Å thick. This interfacial layer has a slightly different composition, as determined from EDS fitted to the transmission electron microscope: it contains about 5% gallium, whereas no gallium is found in the columnar part of the film. Superlattice growth may still be achievable on these

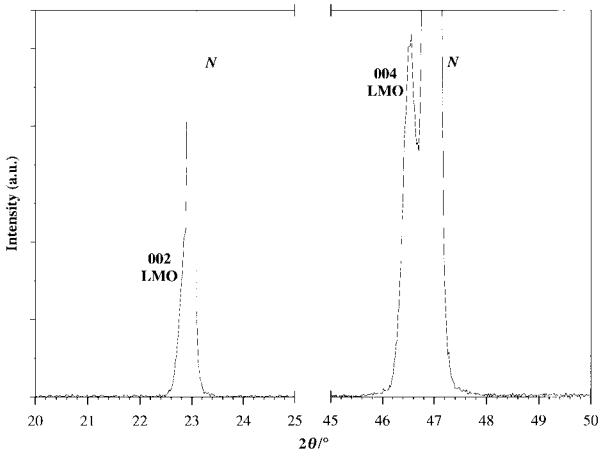

Fig. 5 X-Ray diffraction pattern of a $LaMnO_3$ thin film deposited on a [110]-$NdGaO_3$ substrate. The peaks from the film are indexed as $00l$, $l=2n$, reflections of a perovskite-like structure: the 002-LMO and 004-LMO peaks. The peaks from the [110]-$NdGaO_3$ substrate are denoted by N.

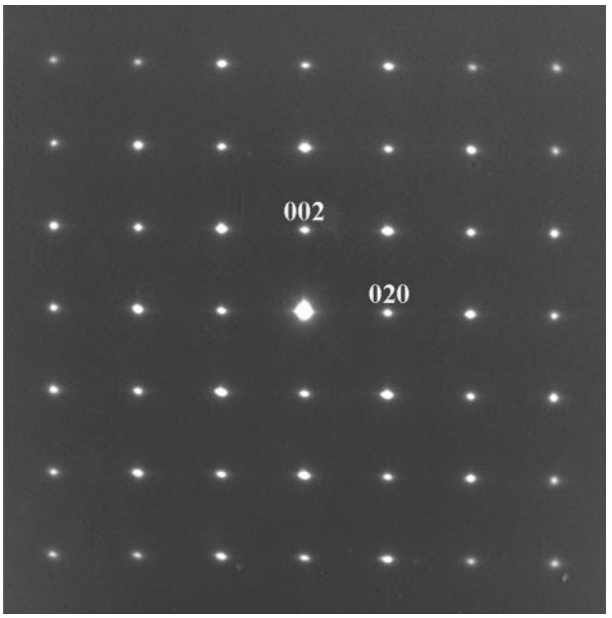

Fig. 6 Electron diffraction pattern viewed along an assumed ***a*** direction of a cross section from a $LaMnO_3$ film deposited on [110]-$NdGaO_3$. The pattern is indexed in the face-centered cell ($2a_p\times 2a_p\times 2a_p$). Deviation from 90° is observable between the $\boldsymbol{c}^*$ and the $\boldsymbol{b}^*$ directions.

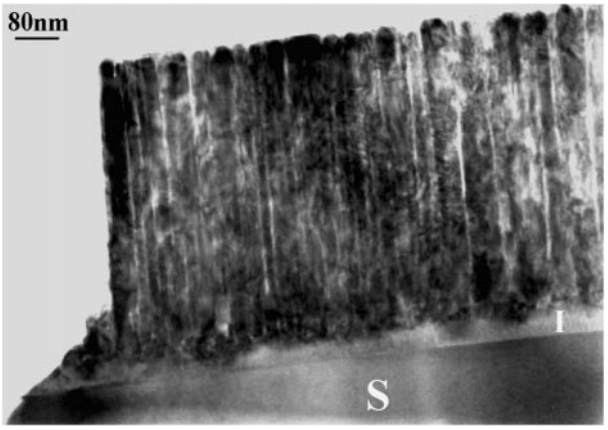

Fig. 7 Low resolution image of the cross-section of a $LaMnO_3$ film on [110]-$NdGaO_3$ evidencing the columnar growth for the majority of the film. The interfacial layer, labeled I, does not have a columnar-like structure and corresponds to a gallium doped (5%) $LaMnO_3$ material. The $NdGaO_3$ substrate is labeled S.

materials because of the uniform height of the columns, but may result in poorly defined interfaces at the grain (column) boundaries.

In contrast to the results obtained for $LaMnO_3$, $SrMnO_3$ films are not stable under similar growth/cooling conditions. No diffraction peaks were observed over the entire range of experimental conditions over which we found $LaMnO_3$ to be well crystallized. Further work is necessary to optimize the growth conditions of this phase as a single material film. Thus, we grew superlattices of $(LMO)_m(YMO)_n$ to demonstrate the feasibility of ordering the A-site cations in non-cuprate perovskites *via* thin film growth.

The X-ray diffraction pattern of such a superlattice, deposited on $LaAlO_3$ using a temperature of 675 °C, a pressure of 0.53 mbar, and cooled in an atmosphere of 500 mbar, is shown in Fig. 8. The observed superlattice period is *ca.* 29.2 Å and the primary peak position is located at $d=3.900$ Å. The superlattice unit thus corresponds to a repeat of 7.5 a_p and to the formula $(LMO)_4(YMO)_{3.5}$, which is in agreement with our observed deposition rates. To calculate a theoretical lattice spacing is somewhat more difficult in the case of the manganese oxides than for the copper oxides. This mainly arises from the fact that the rotations of the manganese-centered octahedra are coupled to the type of epitaxy and this controls the observed lattice spacing. Yet, using the a_p distances of one-

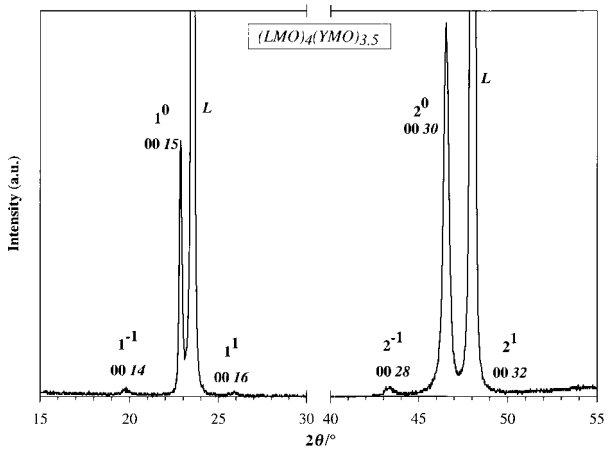

Fig. 8 X-Ray diffraction pattern of the $[(LaMnO_3)_4(YMnO_3)_{3.5}]\times 50$ superlattice film. Intensity is given in arbitrary units. Peaks are indexed according to Schuller's notation (see text) and, alternatively, an expanded unit cell having $c=15a_p$. The peaks from the [100]-$LaAlO_3$ substrate are denoted by *L* .

half the pseudocubic lattice parameter observed above for LMO and one-half the 110 distance of YMO films,[18] the calculated lattice parameter would be 29.22 Å $(4\times 3.898+3.5\times 3.894)$, and a primary peak position at a *d* spacing of 3.986 Å. These values are in close agreement with the observed values.

Note that in cases corresponding to a half-integral coverage of only one layer, the structural periodicity is actually twice that corresponding to the deposition sequence, *i.e.*, in this case 15 perovskite layers and not 7.5, since the doubled distance is the required amount to achieve a true periodic structural alternation.[28,75] The superlattice peaks are therefore labeled accordingly to the structural repeat unit (twice the deposition repeat unit), as shown in Fig. 8. Even in this case where the interfacial layers are mixed owing to the non-integral coverage of the YMO layers, superlattice peaks are observable in the diffraction patterns indicating that a spatial separation of the two A-site cations is achievable in the manganese oxide systems using thin film techniques. More detailed characterizations are required to completely determine the superlattice structural characteristics: particularly, whether or not the columnar growth mode is retained in the sequential deposition process and what are the underlying distortions of the octahedra within each layer and in the interfacial region.

The alternation of LMO and YMO is not the most interesting choice for artificial order from the point of view of attaining colossal magnetoresistant behavior, because they both ideally contain only Mn^{3+} (in the absence of defects) cations. To obtain mixed valency on the manganese sublattice, *i.e.*, Mn^{3+}/Mn^{4+} cations, one would like to alternate $LnMnO_3$ (Ln = lanthanide, Y) and $AEMnO_3$ (AE = alkaline earth) layers (in a similar manner to the bulk compound $LaBaMn_2O_6$[73]). However, we were unable to obtain highly crystalline films of $SrMnO_3$ using similar conditions to those for $LaMnO_3$ (between 600 °C and 700 °C under oxygen pressures of 0.2–0.5 mbar). Typically this implies that stabilization of the superlattices will be difficult. We nevertheless attempted superlattice growth of LMO and SMO in conditions where the SMO films themselves were unstable. Such superlattices, $(LMO)_m(SMO)_n$, were deposited using deposition parameters as above with a temperature of 680 °C, a pressure of 0.53 mbar, and cooled in an atmosphere of 500 mbar. Because $SrMnO_3$ was not found to be stable as a single film, the deposition rate could not be determined prior to superlattice deposition. Thus, superlattice periods and deposition rates were determined by comparison between several different stacking periods deposited under similar conditions.

The diffraction pattern from two such films are given in Fig. 9 and 10. The diffraction spectrum shown in Fig. 9 corresponds well to a material having the stoichiometry $[(LMO)_{7.5}(SMO)_4]\times 50$, *i.e.*, $m=7.5$ and $n=4$. Films deposited on both $NdGaO_3$ and $LaAlO_3$ exhibit satellite peaks around both primary reflections from the basic perovskite cell. Again, even with a mixed interfacial region, the diffraction data evidence periodic separation of the A-site cations. In Fig. 10, satellite peaks are observed in the diffraction pattern for a superlattice having a thinner layer of $SrMnO_3$, *i.e.*, $[(LMO)_{7.5}(SMO)_2]\times 50$, deposited on $LaAlO_3$. The primary peak position is correspondingly shifted closer to that of LMO for the latter superlattice (although without a definite lattice parameter for $SrMnO_3$ under these synthesis conditions). In both cases the superlattices are indexed on a repeat distance twice as long as the half-integral deposition sequence: $\Lambda=44.3$ ($\approx 11.5\ a_p$), for $m=7.5$, $n=4$; and $\Lambda=37.3$ ($\approx 9.5\ a_p$), for $m=7.5$, $n=2$.

It is interesting to note that these superlattices exhibit good crystalline quality and superlattice peaks despite the instability of one of the structural blocks under the synthesis conditions. This implies that the $SrMnO_3$ perovskite-like layer is stabilized by its spatial confinement between two $LaMnO_3$ blocks.

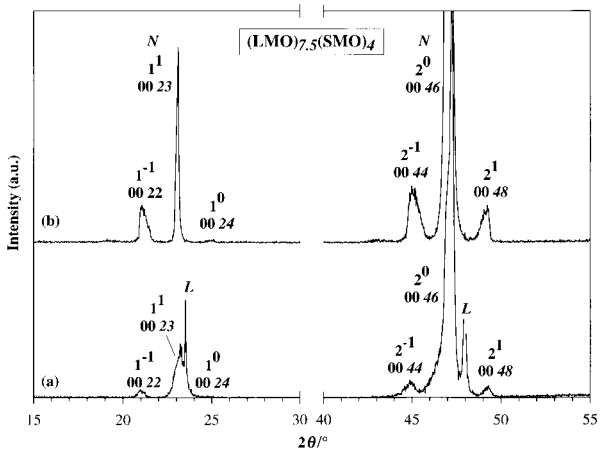

Fig. 9 X-Ray diffraction patterns of the $[(LaMnO_3)_{7.5}(SrMnO_3)_4]\times 50$ superlattice films on (a) a [100]-$LaAlO_3$ substrate and (b) a [110]-$NdGaO_3$ substrate. Intensity is given in arbitrary units. Peaks are indexed according to Schuller's notation (see text) and, alternatively, an expanded unit cell having $c=23a_p$. The peaks from the substrates are denoted by L and N in (a) and (b), respectively.

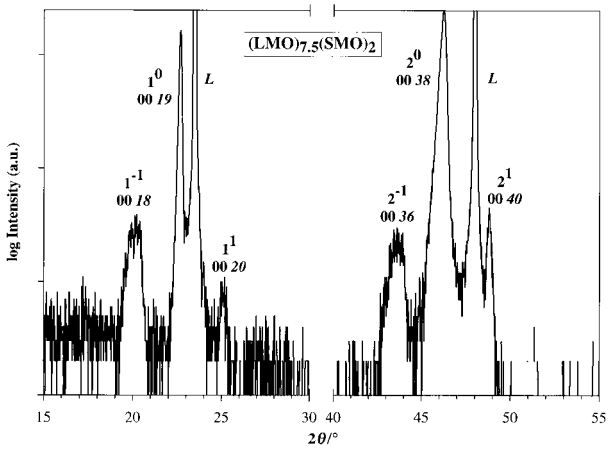

Fig. 10 X-Ray diffraction pattern of the $[(LaMnO_3)_{7.5}(SrMnO_3)_2]\times 50$ superlattice film on a [100]-$LaAlO_3$ substrate. Intensity is given on a logarithmic unit in arbitrary units. Peaks are indexed according to Schuller's notation (see text) and, alternatively, an expanded unit cell having $c=19a_p$. The peaks from the substrate are denoted by L.

Similar superlattice stabilization owing to structural/chemical factors was mentioned above with respect to the excess oxygen in the SCO layers of the LBCO/SCO superlattices, and this is in general not surprising from a chemical point of view. Further work is necessary to understand completely the nature of these stabilization mechanisms, structural or chemical, but they imply that this synthetic method can be applied to a much larger range of compounds than simply those that exist as stable single-material films, an advantage that may be exploited for the synthesis of a wide range of new chemically tailored materials. The strong chemical stabilizing forces, such as valence mixing between layers, oxygen stoichiometry changes resulting from layer alternation, and interlayer stresses can all contribute to the stability (or instability) of novel materials. Research in this area has focused primarily on the stacking of stable units, however it is clear that further research will lead to new, highly metastable materials and interesting physicochemical properties.

To demonstrate that interesting physical properties can be attained owing to the growth of artificially layered materials, the magnetoresistant behavior of the two LMO/SMO superlattices, which were deposited on $LaAlO_3$ substrates and discussed above, is given in Fig. 11, where the resistivity is given *versus* temperature on both heating and cooling and in applied magnetic fields of 0 and 7 T for both materials. To compare these superlattices to classical materials we must find an approximate stoichiometry for these superlattices: for the $m=7.5$, $n=2$ compound the overall stoichiometry is approximately $La_{0.79}Sr_{0.21}MnO_3$, while for the $m=7.5$, $n=4$ compound the overall stoichiometry is approximately $La_{0.65}Sr_{0.35}MnO_3$. For both superlattices we observe CMR effects of the order of 50–100%. For the $m=7.5$, $n=2$ superlattice [Fig. 11(a)] we observe normal CMR behavior, that is to say an insulator–metal transition, when $B=0$ T, at a temperature $T_{MI}(B=0\text{ T})\approx 240$ K which shifts to a higher value on the application of an applied field, in this case $T_{MI}(B=7\text{ T})\approx 290$ K. A corresponding ferromagnetic transition was observed at the insulator–metal transition temperature in the DC magnetization *vs.* temperature data (not shown). This zero-field transition temperature is slightly shifted from the bulk value, $T_{MI}(B=0\text{ T})\approx 300$ K, for a material with a similar overall composition.[83]

More surprising, however, is the behavior of the $m=7.5$, $n=4$ sample [Fig. 11(b)]: in particular, the occurrence of several distinct regions/transitions of the resistivity with temperature. While the overall CMR effect is weaker in this sample compared to the prior superlattice, it is observed over the entire temperature range below a first insulator–metal transition [$T_{MI}(B=0\text{ T})\approx 265$ K; $T_{MI}(B=7\text{ T})\approx 310$ K]. This first insulator–metal transition is similar to the normal CMR transition, and a paramagnetic–ferromagnetic transition is seen in the DC magnetization (not shown) at a similar temperature. As with the previous superlattice, this transition is shifted

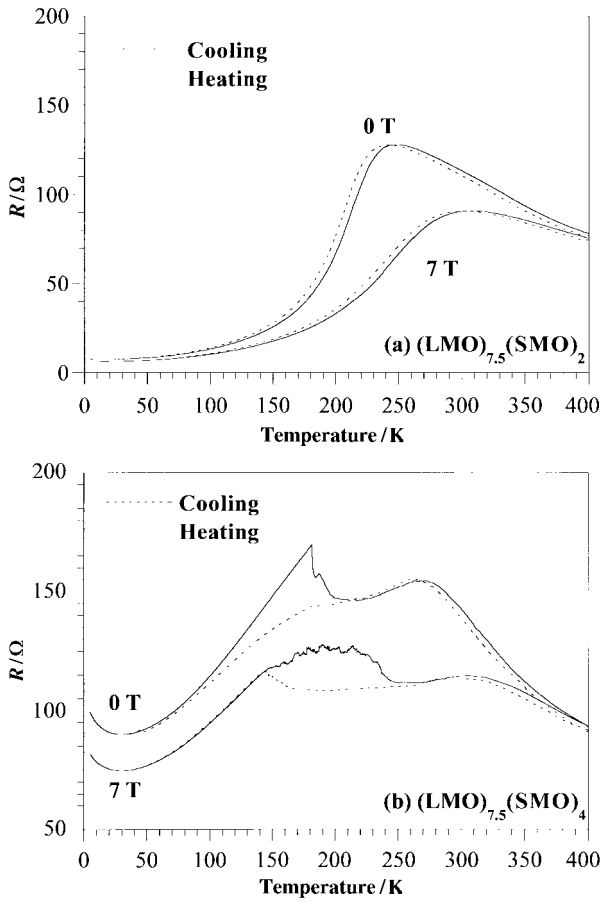

Fig. 11 Resistance *versus* temperature on heating and cooling in no applied magnetic field (0 T) and in an applied magnetic field of 7 T for the superlattices (a) $(LaMnO_3)_{7.5}(SrMnO_3)_2$ and (b) $(LaMnO_3)_{7.5}(SrMnO_3)_4$, both on [100]-$LaAlO_3$.

to lower temperature with respect to the expected value [$T_{MI}(B=0\ T)\approx 350\ K$] for a material of this stoichiometry.[83]

The metal-like resistivity (decreasing resistivity with decreasing temperature) is not observed over a large range of temperature below this transition. A region of very weak dependence of the resistivity on temperature is observed before a second transition occurs to another metallic state. This second transition shows a strong temperature hysteresis between the cooling and heating curves. Particularly in the data for $B=7$ T, the heating and cooling resistivity curves diverge over a temperature range of nearly 80 K. The structural origin of this behavior cannot be understood from the current data alone, but it appears to be related to the unique stacking sequence obtained with this synthetic approach. While we cannot rule out microstructural effects as an origin for this behavior, the stacking sequence/stoichiometry appears to play a more prominent role since this behavior is not observed in the superlattice with a thinner layer of $SrMnO_3$. We are currently pursuing further experiments to understand the physical basis and structural origin of these transitions. A final metal to insulator transition is observed at lower temperatures, *ca.* 30 K at both 0 T and 7 T. While the transition temperature is only weakly field-dependent, the overall resistivity values are field-dependent over the entire low temperature regime.

4. Conclusions

The complexity of the charge, orbital, magnetic and structural interactions in the manganese and copper based perovskites renders determination of the physical origin of the observed physical properties beyond the scope of the current paper, which has focused on the synthesis of novel materials. Previous work on PLD superlattice growth has focused predominantly on materials having extremely similar structures and chemistries. A variety of new materials having designed, artificial cationic-order may not, however, fall into this category. Much work is required to extend thin film deposition techniques to include the synthesis of these other types of tailored materials. In addition to reviewing briefly the PLD synthetic approach, as well as other thin-film deposition techniques, we have discussed several examples to demonstrate the applicability of this approach to the synthesis of a wider class of materials, whose structures may be unstable as single material films, such as $SrMnO_3$, or whose structural chemistry is changed as a result of superlattice formation, such as the incorporation of excess oxygen in LBCO/SCO superlattices. These materials were indeed stabilized as superlattices, indicating that PLD synthesis of novel materials is only in its early stages of development, and that many new materials can be stabilized which may have interesting properties.

The biggest drawback to the standard PLD synthesis of artificial structures is the lack of precision on the absolute period of the superlattices. Although we have stabilized compositional modulations in the $(LBCO)_m(SCO)_n$ and $(LMO)_m(AMO)_n$ systems, their structural quality and microstructure/defect structure need to be further investigated and optimized. Synthetic techniques which allow for *in-situ* control over the layer thicknesses will greatly enhance the structural quality of the superlattices. As discussed in section 1.2, laser-MBE allows for just this type of control using lower deposition pressures to allow for the incorporation of reflection high energy electron diffraction (RHEED) to monitor the growth.[13,14,30,38–42,46] Several superlattices have been grown using this approach, although a great deal more work is required in order to completely understand the growth and oxidation mechanisms in this low-pressure deposition environment. It is, however, a promising, powerful approach to the synthesis of artificially layered materials having excellent crystal qualities.

The usefulness of thin-film deposition is currently being extended outside the area of technologically useful forms of materials, and into the area of novel materials synthesis and atomic-structure engineering. While a small body of exciting and impressive results have already been obtained, this approach promises to be an indispensable tool for the development of a wide variety of advanced materials.

The authors would like to thank M. Strobel for the preparation of the sample for the cross-sectional electron microscopy study. P.A.S. gratefully acknowledges the financial support of the Chateaubriand Fellowship and CNRS.

References

1 *Handbook of Thin Films Technology*, ed. L. I. Maissel and R. Glang, McGraw-Hill, New York, 1970.
2 M. A. Herman and H. Sitter, *Molecular Beam Epitaxy: Fundamentals and Current Status*, Springer-Verlag, Berlin, 1989.
3 D. Diijkamp, T. Venkatesan, X. D. Wu, S. A. Shaheen, N. Jinawi, Y. H. Minke-Lee, W. L. McLean and M. Croft, *Appl. Phys. Lett.*, 1987, **51**, 619.
4 F. S. Galasso, *Perovskites and High T_c Superconductors*, Gordon and Breach Science Publishers, New York, 1990.
5 B. Raveau, C. Michel, M. Hervieu and D. Groult, *Crystal Chemistry of High-T_c Superconducting Copper Oxides*, Springer-Verlag, Berlin, 1991.
6 T. Kawai, Y. Egami, H. Tabata and S. Kawai, *Nature,* 1991, **349**, 200.
7 C. Niu and C. M. Lieber, *J. Am. Chem. Soc.*, 1992, **115**, 137.
8 J. N. Eckstein and I. Bozovic, *Ann. Rev. Mater. Sci.,* 1995, **25**, 679.
9 I. Bozovic and J. N. Eckstein, in *Physical Properties of High Temperature Superconductors V*, ed. D. M. Ginsberg, World Scientific, Singapore, 1996, p. 99.
10 V. Matijasevic and I. Bozovic, *Curr. Opin. Solid State Mater. Sci.*, 1996, **1**, 47.
11 H. Adachi, M. Sakai, T. Satoh and K. Setsune, *Proceedings from 8th International Symposium on Superconductivity*, ed. H. Hayakawa and Y. Enomoto, Hamamatsu, 1995, p. 955.
12 D. H. Lowndes, D. B. Goehegan, A. A. Puretzky, D. P. Norton and C. M. Rouleau, *Science*, 1996, **273**, 898.
13 A. Gupta, *Curr. Opin. Solid State Mater. Sci.*, 1997, **2**, 23.
14 J. F. Hamet and B. Mercey, *Curr. Opin. Solid State Mater. Sci.*, 1998, **3**, 144.
15 H. Sellinschegg, S. L. Stuckmeyer, M. D. Hornbostel and D. C. Johnson, *Chem. Mater.*, 1998, **10**, 1096.
16 D. C. Johnson, *Curr. Opin. Solid State Mater. Sci.,* 1998, **3**, 159.
17 L. Niinistö, *Curr. Opin. Solid State Mater. Sci.,* 1998, **3**, 147.
18 P. A. Salvador, T.-D. Doan, B. Mercey and B. Raveau, *Chem. Mater.*, in press.
19 N. Sugii, M. Ichikawa, K. Hayashi, K. Kubo, K. Yamamoto and H. Yamauchi, *Physica C*, 1993, **213**, 345.
20 E. Koller, L. Miéville, G. Triscone, J. Cors, J. M. Triscone and O. Fischer, *J. Alloys Compd.*, 1993, **195**, 303.
21 T. Satoh, H. Adachi, Y. Ichikawa, K. Setsune and K. Wasa, *J. Mater. Res.*, 1994, **8**, 1961.
22 H. Adachi, T. Satoh, M. Sakai, K. Mizuno and K. Setsune, *J. Supercond.*, 1994, **7**, 737.
23 J. M. Triscone, M. G. Karkut, L. Antognazza, O. Brunner and O. Fischer, *Phys. Rev. Lett.*, 1989, **63**, 1016.
24 J. M. Triscone, O. Fischer, L. Antognazza, A. D. Kent and M. G. Karkut, *Phys. Rev. Lett.*, 1990, **64**, 804.
25 G. Jakob, T. Hahn, T. Kluge, P. Wagner and H. Adrian, *J. Supercond.*, 1994, **7**, 197.
26 Y. Suzuki, J. M. Triscone, C. B. Eom, M. R. Beaseley and T. H. Geballe, *Phys. Rev. Lett.*, 1994, **73**, 328.
27 Z. Z. Li, H. Rifi, A. Vaures, S. Megtert and H. Raffy, *Phys. Rev. Lett.*, 1994, **73**, 328.
28 K. Nakamura and T. Hatano, *J. Appl. Phys.*, 1995, **77**, 6402.
29 H. Adachi, M. Sakai, T. Satoh and K. Setsune, *Physica C*, 1996, **261**, 295.
30 K. Iijima, T. Terashima, Y. Bando, K. Kamigaki and H. Terauchi, *J. Appl. Phys.*, 1992, **72**, 2840.
31 J. N. Eckstein, I. Bozovic, M. E. Klausmeier-Brown, G. F. Virshup and K. S. Ralls, *Thin Solid Films*, 1992, **216**, 8.
32 J. Lesueur, M. Aprili, A. Goulon, T. J. Horton and L. Dumoulin, *Phys. Rev. B*, 1997, **55**, R3398.
33 J. P. Locquet, Y. Jaccard, C. Gerber and E. Mälcher, *Appl. Phys. Lett.*, 1993, **63**, 1426.

34 J. P. Locquet, A. Cantana, E. Mälcher, C. Gerber and J. G. Bednorz, *Appl. Phys. Lett.*, 1994, **64**, 372.
35 H. Yamamoto, M. Naito and H. Sato, *Jpn. J. Appl. Phys.,* 1997, **36**, L341.
36 I. Bozovik and J. N. Eckstein, *Proceedings from 10th Anniversary HTS Workshop: Physics, Materials and Applications*, ed. B. Batlogg, C. W. Chu, W. K. Chu, D. U. Gubser and K. A. Müller, World Scientific, Singapore, 1996, p. 145.
37 J. N. Eckstein, I. Bozovic, J. O'Donnell, M. Oneillon and M. S. Rzchowski, *Appl. Phys. Lett.*, 1996, **69**, 1312.
38 M. Yoshimoto, H. Nagata, J. Gong, H. Ohkubo and H. Koinuma, *Physica C*, 1991, **185–189**, 2085.
39 M. Yoshimoto, H. Ohkubo, N. Kanda, H. Koinuma, K. Horiguchi, M. Kumagai and K. Hirai, *Appl. Phys. Lett.*, 1992, **61**, 2659.
40 T. Kawashima, Y. Matsui and E. Takayama-Muromachi, *Physica C*, 1994, **224**, 69.
41 A. Gupta, B. W. Hussey, T. M. Shaw, A. M. Guloy, M. Y. Chern, R. F. Saraf and B. A. Scott, *J. Solid State Chem.,* 1994, **112**, 113.
42 A. Gupta, T. M. Shaw, M. Y. Chern, B. W. Hussey, A. M. Guloy and B. A. Scott, *J. Solid State Chem.*, 1995, **114**, 190.
43 H. Koinuma, M. Kawasaki and M. Yoshimoto, *Proceedings from Materials Research Society Meeting*, vol. 397, ed. R. Singh, D. Norton, L. Lande, J. Narayan and J. Chueng, Materials Research Society, Warrendale, 1996, 145.
44 X. Li, T. Kawai and S. Kawai, *Jpn. J. Appl. Phys.,* 1994, **33**, L18.
45 T. Maeda, M. Yoshimoto, K. Shimozono and H. Koinuma, *Physica C*, 1995, **247**, 142.
46 I. Kawayama, M. Kanai and T. Kawai, *Jpn. J. Appl. Phys.,* 1996, **35**, L926.
47 A. Tsukamoto, J. G. Wen, K. Nakanishi and K. Tanabe, *Physica C*, 1997, **292**, 17.
48 S. Matunarai, M. Kanai and T. Kawai, *Jpn. J. Appl. Phys.*, 1995, **34**, L20.
49 S. Matunarai, M. Kanai and T. Kawai, *Physica C*, 1995, **253**, 217.
50 *Pulsed Laser Deposition of Thin Films*, ed. D. B. Chrisey and G. K. Hubler, John Wiley & Sons, New York, 1994.
51 T. Kawai, M. Kanai and H. Tabata, *Mater. Sci. Eng. B*., 1996, **41**, 123.
52 H. Tabata and T. Kawai, *IEICE Trans. Electron.*, 1997, **E80-C**, 918.
53 H. Tabata and T. Kawai, *Appl. Phys. Lett.*, 1997, **70**, 231.
54 Z. W. Dong, R. Ramesh, T. Venkatesan, M. Johnson, Z. Y. Chen, S. P. Pai, V. Talyansky, R. P. Sharma, R. Shreekala, C. J. Lobb and R. L. Greene, *Appl. Phys. Lett.*, 1997, **71**, 1718.
55 A. Gupta, B. Mercey, M. Hervieu and B. Raveau, *Chem. Mater.*, 1994, **6**, 1011.
56 R. Desfeux, J. F. Hamet, B. Mercey, C. Simon, M. Hervieu and B. Raveau, *Physica C*, 1994, **221**, 205.
57 C. Michel, L. E. Rakho, M. Hervieu, J. Pannetier and B. Raveau, *J. Solid State Chem.*, 1987, **68**, 143.
58 J. L. Allen, B. Mercey, W. Prellier, J. F. Hamet, M. Hervieu and B. Raveau, *Physica C*, 1995, **241**, 158.
59 D. P. Norton, J. D. Budai, D. H. Lowndes and B. C. Chakoumakos, *Appl. Phys. Lett.*, 1994, **65**, 2869.
60 C. Aruta, G. Balestrino, R. Desfeux, S. Martellucci, A. Paoletti and G. Petrocelli, *Appl. Phys. Lett.*, 1996, **68**, 926.
61 F. Arciprete, G. Balestrino, S. Martelluci, P. G. Medaglia, A. Paoletti and G. Petrocelli, *Appl. Phys. Lett.*, 1997, **71**, 959.
62 W. Prellier, B. Mercey, P. Lecoeur, J. F. Hamet and B. Raveau, *Appl. Phys. Lett.*, 1997, **71**, 782.
63 E. Wiener-Avnear, *Appl. Phys. Lett.*, 1994, **65**, 1784.
64 H. Tabata, H. Tanaka and T. Kawai, *Appl. Phys. Lett.,* 1994, **65**, 1970.
65 H. M. Christen, L. A. Boatner, J. D. Budai, M. F. Chicholm, L. A. Géa, P. J. Marrero and D. P. Norton, *Appl. Phys. Lett.*, 1996, **68**, 1488.
66 M. Y. Chern, C. C. Fang, J. S. Liaw, J. G. Lin and C. Y. Huang, *Appl. Phys. Lett.*, 1996, **69**, 854.
67 J. D. Jorgensen, D. G. Hinks, O. Chmaissem, D. N. Argyriou, J. F. Mitchell and B. Dabrowski, in *Recent Developments in High Temperature Superconductivity*, ed. J. Klamut, B. W. Veal, B. M. Dabrowski, P. W. Klamut and M. Kazimierski, Springer-Verlag, Berlin, 1996, p. 1.
68 P. A. Salvador, T. O. Mason, M. E. Hagerman and K. R. Poeppelmeier, in *Chemistry of Advanced Materials: An Overview*, ed. L. V. Interrante and M. Hampden-Smith, Wiley-VCH, Inc., New York, 1998, p. 449.
69 K. Otzschi, K. Kogi and Y. Ueda, *J. Solid State Chem.,* 1995, **115**, 490.
70 K. Otzschi and Y. Ueda, *J. Solid State Chem.*, 1993, **107**, 149.
71 K. Otzschi, A. Hayashi, Y. Fujiwara and Y. Ueda, *J. Solid State Chem.*, 1993, **105**, 573.
72 P. K. Davies and C. M. Katzan, *J. Solid State Chem.,* 1990, **88**, 368.
73 F. Millange, V. Caignaert, B. Domengès, B. Raveau and E. Suard, *Chem. Mater.*, 1998, **10**, 1974.
74 I. K. Schuller, *Phys. Rev. Lett.*, 1980, **44**, 1597.
75 I. K. Schuller, M. Grimsditch, F. Chambers, G. Devane, H. Vanderstraeten, D. Neerinck, J.-P. Locquet and Y. Bruynseraede, *Phys. Rev. Lett.*, 1990, **65**, 1235.
76 S. Pignard, H. Vincent, J. P. Sénateur and J. Pierre, *J. Alloys Compd.*, 1997, **262–263**, 157.
77 A. Gupta, T. R. McGuire, P. R. Duncombe, M. Rupp, J. Z. Sun, W. J. Gallagher and G. Xiao, *Appl. Phys. Lett.*, 1995, **67**, 3494.
78 T. R. McGuire, A. Gupta, P. R. Duncombe, M. Rupp, J. Z. Sun, R. B. Laibowitz and W. J. Gallagher, *J. Appl. Phys.,* 1996, **79**, 4549.
79 H. N. Aiyer, A. R. Raju, G. N. Subbanna and C. N. R. Rao, *Chem. Mater.*, 1997, **9**, 755.
80 S. S. Manoharan, D. Kumar, M. S. Hegde, K. M. Satyalakshmi, V. Prasad and S. V. Subramanyam, *J. Solid State Chem.*, 1995, **117**, 420.
81 M. Hervieu, R. Mahesh, N. Rangavittal and C. N. R. Rao, *Eur. J. Solid State Inorg. Chem.*, 1995, **32**, 79.
82 J. Töpfer and J. B. Goodenough, *Chem. Mater.*, 1997, **9**, 1467.
83 A. Urushibara, Y. Morimoto, T. Arima, A. Asamitsu, G. Kido and Y. Tokura, *Phys. Rev. B*, 1995, **51**, 14103.

Paper 8/04929G